Appl. Sci. Converg. Technol. 30 (2); 45-49 (2021)
https://doi.org/10.5757/ASCT.2021.30.2.45

eISSN: 2288-6559

ASCT Applied Science and Convergence Technology

Research Paper Check for updates

Universal Transfer of 2D Materials Grown on Au Substrate Using Sulfur Intercalation

Received 8 December, 2020; revised 21 January, 2021; accepted 26 January, 2021

Soo Ho Choi[a], Ji Hoon Choi[b], Chang Seok Oh[b], Gyeongtak Han[b], Hu Young Jeong[c], Young-Min Kim[a,b], Soo Min Kim[d,*], and Ki Kang Kim[a,b,*]

[a]Center for Integrated Nanostructure Physics (CINAP), Institute for Basic Science (IBS), Sungkyunkwan University, Suwon 16419, Republic of Korea
[b]Department of Energy Science, Sungkyunkwan University, Suwon 16419, Republic of Korea
[c]UNIST Central Research Facilities and Department of Materials Science and Engineering, UNIST, Ulsan 44919, Republic of Korea
[d]Department of Chemistry, Sookmyoung Women's University, Seoul 14072, Republic of Korea

*Corresponding author E-mail: kikangkim@skku.edu, soominkim@sookmyung.ac.kr

ABSTRACT

Herein, we report on a novel method for transferring two-dimensional (2D) materials grown on Au substrates using sulfur intercalation between the 2D materials and the Au surfaces. The strong nature of the S–Au bond allows intercalation of sulfur atoms into their interface, under a sulfur-rich atmosphere, at 600 °C. The relaxed interfacial interaction achieved via intercalation is carefully confirmed by recovering phonon mode and work function of tungsten disulfide (WS_2) in Raman spectra and Kelvin probe force microscopy, and, more importantly, by observing the expansion of the interfacial distance, from 0.24 to 0.44 nm, using cross-sectional transmission electron microscopy. The released interactions facilitate delamination of WS_2 from the Au surface, using an electrochemical bubbling method. The resultant Au foil then is reused for repeated WS_2 growth. The successful transfer of other 2D materials, including molybdenum disulfide and hexagonal boron nitride, is also demonstrated. Our strategy advances the use of Au substrates for growing wafer-scale 2D monolayers.

Keywords: Two-dimensional materials, Transition metal dichalcogenides, Chemical vapor deposition, Gold, Intercalation

1. Introduction

Interest in two-dimensional (2D), van der Waals (vdW) layered materials, including graphene (Gr), transition metal dichalcogenides (TMDC), and hexagonal boron nitride (hBN), has recently increased, owing to their unusual physical and chemical properties [1–6]. To utilize those emerging materials into industrial applications, wafer-scaled growth of 2D materials is highly desired. Among various growth techniques including molecular beam epitaxy, atomic layer deposition, puls -ed layer deposition, and chemical vapor deposition (CVD) [7–10], CVD method has been mostly employed, due to its several advantages compared to other growth techniques, which include mass production, cost-effectiveness, and low temperature operation.

The substrate is most important key ingredient for the CVD growth of 2D materials to control morphology, orientation, and growth modes [10–22]. While chemically stable insulating substrates such as SiO_2, Al_2O_3, glass, and quartz enable to grow the various poly-crystalline TMDCs film, the lack of catalytic activity impedes the synthesis of Gr and hBN film. On the other hand, the catalytic metal substrates such as Cu, Ni, and Fe have been widely exploited for the growth of Gr and hBN, but the high chemical reactivity with chalcogens and transition metals to form alloy and compound, prohibits to use as the growth substrate for TMDCs. To date, only Au metal can serve as universal growth substrate for most of 2D materials owing to possessing the unique characteristics of high chemical inertness (that is, no alloy and compound formation), scarce B, N, S, and transition metal solubilities in bulk Au, and its ability to act as a catalyst for activating precursors.

Recently, wafer-scale, single-crystal (SC) 2D films such as hBN, WS_2, MoS_2, WSe_2, $MoSe_2/WSe_2$ lateral heterostructure, and $W_{1-x}Mo_x-S_2$ alloy have been successfully synthesized on Au foil, using the self-collimation and epitaxial growth methods [16, 20]. When using SC 2D materials in practical device applications, it inevitably becomes necessary to transfer 2D film onto other substrates. CVD-grown 2D materials are typically transferred after wet-etching the growth substrate. For example, Cu foils used for graphene growth have typically been etched away in etchant solution [21], while for more costly Au foils, non-destructive methods, such as electrochemical bubble transfers, have been more popular than wet-etching process. A few studies have reported transferring 2D material grown on Au foils via electrochemical bubbling [16,18], although it was found that the strong Au–S interaction reduced the efficiency with which 2D materials could be detached from the Au surface during electrochemical bubbling, leading to poor transfer yields [18]. Despite this, it appears that relaxing this strong interfacial interaction to attain a higher transfer yield has not been studied.

Here, we report a universal transfer method for 2D material grown on Au foil, using S-intercalation into the interface between the 2D material and the Au surface. The S-intercalation was carried out by annealing in an S-rich atmosphere, at 600 °C. The interfacial distance between WS_2 and the Au surface had increased, from 0.24 to 0.44 nm, reducing the interfacial interaction. Such relaxed interaction restored the WS_2 electronic structure toward its undoped state, and, more importantly, allowed easy WS_2 film delamination from the Au surface, using electrochemical bubbling. Eventually, the cm-scale WS_2 film

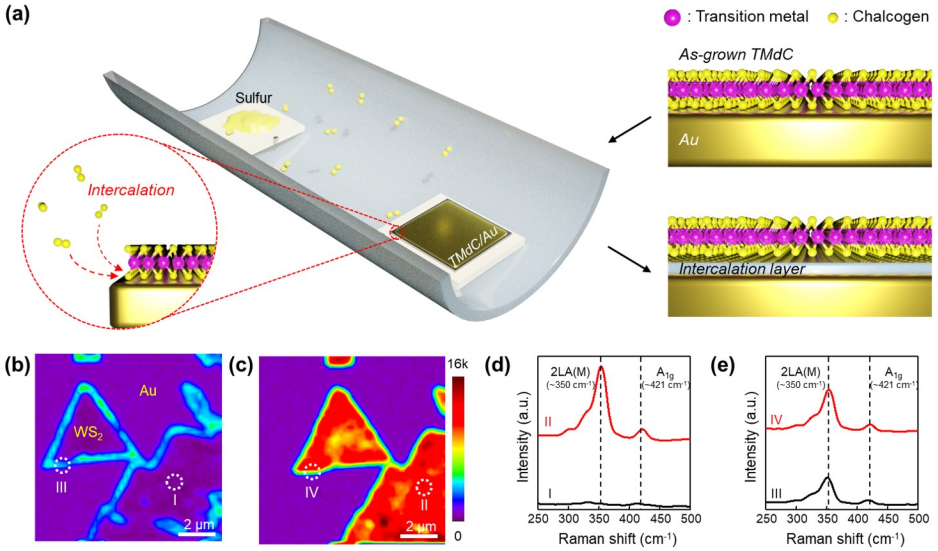

Figure 1. (a) Schematic of the intercalation process. The S atoms are intercalated between the TMdC and Au layers, under an S-rich atmosphere, at 600 °C. Confocal Raman mapping images of (b) as-grown and (c) intercalated WS_2 grains, for 2LA(M) mode intensity. (d) and (e) Representative Raman spectra extracted from regions I–IV in (b) and (c).

was successfully transferred onto a SiO_2 substrate. Importantly, we have also shown that the Au foils could be reused for repeated WS_2 growth cycles, and have demonstrated the effective transfers of monolayer MoS_2 and hBN grown on Au substrates.

2. Experimental details

2.1. Substrate preparation

1 × 1 cm^2, high-purity Au foils (0.2 mm thick, 99.99 %, iNexus Inc.) were cleaned using ultra-sonication in acetone and isopropyl alcohol respectively, for 30 s. The surface impurities on Au substrates were then removed by dipping into Au etchant (GE-8111, Transene), for 10 min. The etchant residue was rinsed away using deionized (DI) water, and the Au foils were then further annealed, at 1000 °C for 1 h, under Ar and H_2 atmospheres with flow rates of 1000 and 50 sccm, respectively. To obtain smooth surfaces, the Au foils were melted onto a W foil (0.1-mm thick, 99.95 %, Alfa Aesar), at 1080 °C for 20 min, under the same conditions. All the experiments in this work were conducted at atmospheric pressure.

2.2. Growing TMDC monolayers

WS_2 monolayer growth was carried out through sulfurization of tungsten precursor-coated Au substrates [16]. The W precursor was prepared by dissolving 2 wt% sodium tungstate dihydrate in acetylacetone. The prepared solution was spun onto an Au substrate, at 2500 rpm for 60 s, and an ammonium sulfide [$(NH_4)_2S$] solution, acting as a sulfur precursor, was supplied, using a bubbler system [22]. The precursor-coated Au substrate was then loaded into a 2-inch quartz tube—which had been purged for 15 min using high-purity (99.9999 %) Ar, with a flow rate of 350 sccm—and placed into a furnace. The temperature of the furnace containing the quartz tube was increased to 800 °C, over 10 min, and was then maintained at this temperature for 15 min, for WS_2 growth. This growth took place under an H_2 and $(NH_4)_2S$ atmosphere, supplied at flow rates of 5 and 20 sccm, respectively. After the growth process, the quartz tube was naturally cooled to room temperature. Monolayer MoS_2 flakes were grown under conditions similar to those applied for WS_2 growth, except that sodium molybdate was used as the Mo precursor.

2.3. Growing hBN monolayers

The hBN monolayer growth method was described in our previous report [16]. Briefly, Au foil stacked on W foil was mounted into a 1-inch quartz tube in a furnace. The temperature was elevated to 1100 °C, under Ar and H_2 with flow rates of 500 and 40 sccm, to establish liquid Au on the W foil, and then borazine was supplied (as the hBN precursor) for 10 min, at the flow rate of 0.4 sccm. After hBN grains had been grown, the furnace was rapidly cooled to room temperature.

2.4. S-intercalation

A two-zone furnace system was used for the sulfur intercalation process. The upstream and downstream zones were used to vaporize sulfur powder, and to provide the thermal energy for sulfur intercalation, respectively. Then, 1 g of sulfur powder, contained in a quartz boat, and as-grown 2D materials on Au substrate, were loaded into the center of each zone. To avoid any damage to the 2D materials during S-intercalation, the quartz tube was completely purged initially, by supplying Ar gas with a flow rate of 500 sccm, for 30 min. The temperatures in the two zones were increased to 340 and 600 °C for 15 min, and then maintained at these levels for 30 min. After finishing S-intercalation, the temperatures were allowed to lower naturally, to room temperature. The entire process was conducted under Ar and H_2 atmospheres, at flow rates of 300 and 10 sccm, respectively, and at atmospheric pressure.

2.5. Electrochemical Transfer

The poly(methyl methacrylate) (A9 PMMA, MicroChem) layer was spun as the supporting layer onto the 2D material, at 4000 rpm for 60 s, and then dried in a 200 °C oven for 5 min. For an electrochemical transfer, the sample and Pt foil were connected to cathode and anode, respectively, in a power supply [20]. The PMMA/2D material layer was delaminated from the Au surface using generated H_2 bubbles under an applied voltage of 3–10 V, in 1 M NaOH electrolyte. NaOH residues underneath the PMMA/2D material layer were removed by floating on DI water several times, before, the PMMA/2D material layer was transferred onto a SiO_2/Si substrate. To reuse Au substrates, they were cleaned—by dipping in piranha solution for 3–5 h, 10 %

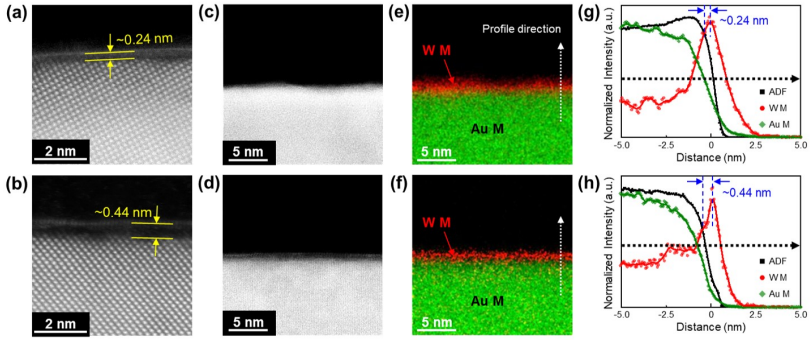

Figure 2. Cross-sectional ADF-STEM images of WS_2 on Au foil (a) and (c) before, and (b) and (d) after S-intercalation, with (e) and (f) showing corresponding EDX element mapping images. (g) and (h) EDX intensity profiles along the white-dashed arrows in (e) and (f), respectively.

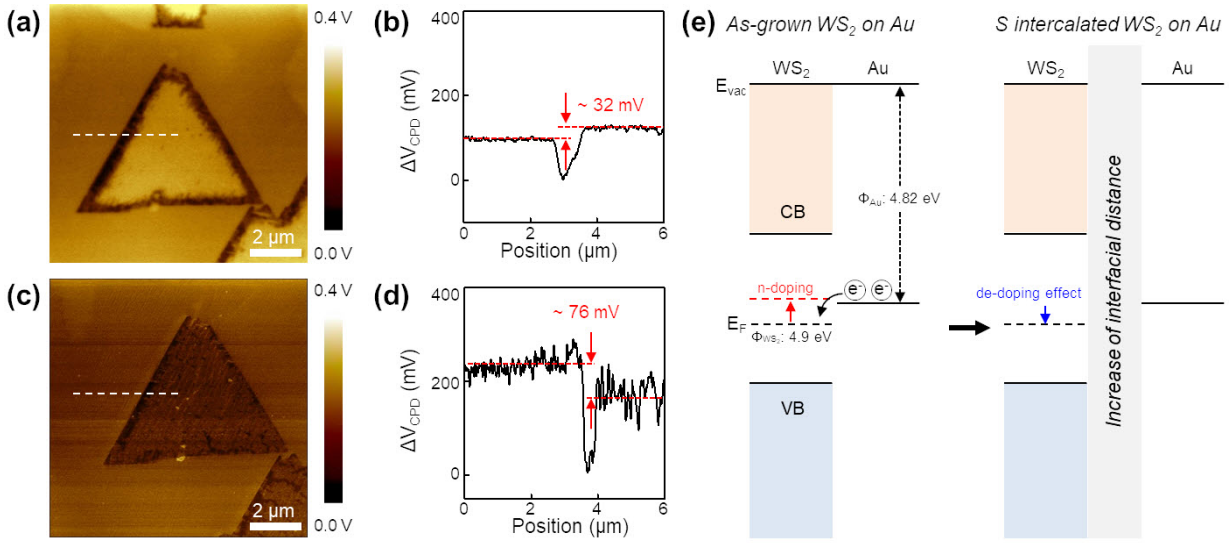

Figure 3. KPFM potential images of (a) as-grown and (c) S-intercalated WS2. (b) and (d) show KPFM potential profiles along the white-dashed lines seen in (a) and (c), respectively. (e) Energy band diagrams for WS_2 and Au substrate, before and after S-intercalation.

nitric acid for 30 min, and buffer oxide etchant for 30 min—prior to being reused.

2.6. Characterization

Overall morphologies of the TMDC and hBN monolayers on Au foil were characterized by field emission scanning electron microscopy (FE-SEM, JSM-7100F, JEOL) and optical microscopy (Eclipse LV150, Nikon). The cross-sectional structures and interlayer distance between WS_2 and Au surface were analyzed using an aberration-corrected scanning transmission electron microscopy (STEM, JEM-ARM 200CF, JEOL), on the samples prepared by a focused ion beam (FIB, FEI Helios NanoLab 450) milling and lift-off process. Modulations of the interfacial interaction and the electronic structure by the S-intercalation were confirmed using Raman spectroscopy with a laser wavelength of 532 nm (XperRAM 100, Nanobase), and a Kelvin probe force microscope (KPFM, N8-NEOS, Bruker), equipped with Pt-coated atomic force microscopy (AFM) probes (Multi-75E, Budget Sensors).

3. Results and discussion

To intercalated S atoms, the annealing of as-grown WS_2 on Au foil was conducted in an S-rich atmosphere, at 600 °C, using CVD to evaporate the S atoms [Fig. 1(a)]. To study the effect of S-intercalation on WS_2, samples were characterized using Raman spectroscopy. While the confocal Raman mapping image of as-grown WS_2 samples showed the solid intensity at the triangular WS_2 grain edges [Fig. 1(b)], strong Raman intensities were detected at both the inner and edge regions of the WS_2 grains after S-intercalation [Fig. 1(c)]. The representative center region Raman spectra [I and II in Fig. 1(d)] showed significant Raman intensity enhancement, whereas only marginal change was observed at the edge regions [III and IV in Fig. 1(e)]. Such strong Raman intensity was attributed to the relaxed interfacial interaction between WS_2 and the Au surface. We noted that the optimized intercalation temperature ranged from 500 to 600 °C (not shown here). WS_2 grains were found to be damaged at 700 °C, whereas the intercalation was found to be inefficient at 400 °C. We also found that the evaporation of S powders was more effective than H_2S or $(NH_4)_2S$ (not shown here).

To evaluate the relaxed interfacial interaction, the interfacial distance was measured directly, using cross-sectional, annular dark-field, scanning transmission electron microscopy (ADF-STEM). In the cross-sectional ADF-STEM image, we were able to distinguish the WS_2 layer from the Au surface of as-grown WS_2 quite clearly, as shown in Fig. 2(a). After S-intercalation, the interfacial distance had increased, from 0.24 to 0.44 nm [Fig. 2(b)]. This distance was further confirmed using the energy-dispersive X-ray spectroscopy (EDX) mapping technique.

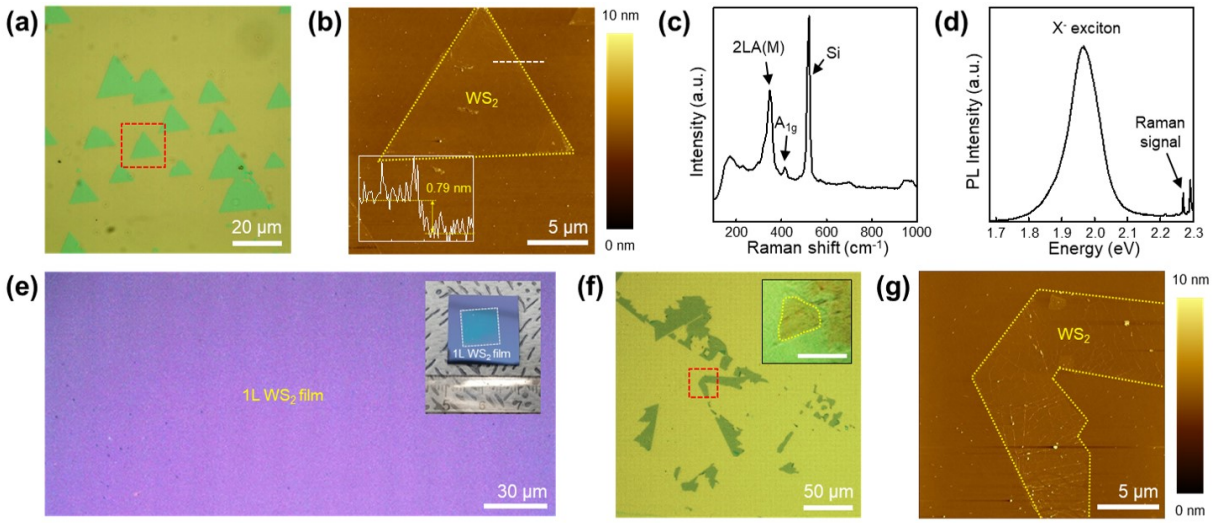

Figure 4. (a) and (b) Optical and AFM topography images of transferred WS_2 grains, after S-intercalation (AFM image was obtained from the red-dashed box, and the inset shows a height profile along the white-dashed line). (c) and (d) Raman and photoluminescence spectra, respectively, for transferred WS_2. (e) Optical image of transferred, cm-scale monolayer WS_2 film, with photograph inset. (f) Optical and (g) AFM topography images of transferred WS_2 grains without S-intercalation. The inset in (f) shows WS_2 grains left on the Au surface after the transfer, and the yellow-dashed line indicates the border line of the leftover WS_2 grains, while the scale bar in the inset of panel (f) represents 10 μm.

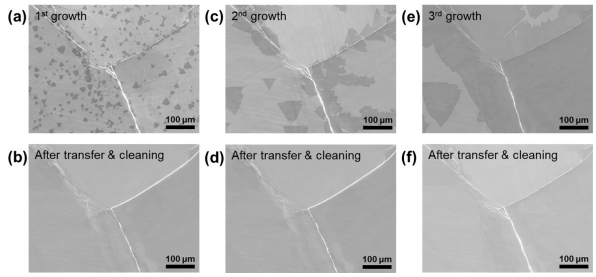

Figure 5. SEM images of WS_2 after the (a) first, (c) second, and (e) third growth processes conducted using the same Au substrate. (b), (d), and (f) are SEM images of the Au substrate after electrochemical transfer and cleaning processes.

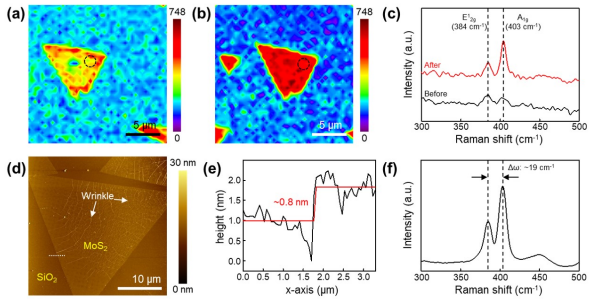

Figure 6. Confocal Raman intensity mapping images of MoS_2 grains (a) before, and (b) after S-intercalation. (c) Raman spectra for MoS_2 extracted from the black-dashed circles in (a) and (b). (d) AFM topography image of transferred MoS_2 grains. (e) Height profile along the white-dashed line in (d). (f) Raman spectrum for a transferred MoS_2 grains.

ADF-STEM and corresponding EDX mapping images of WS_2 samples before and after S-intercalation showed the presence of W and Au elements [Figs. 2(c)–(f)]. We found it difficult to identify the presence of elemental S in the EDX mapping imagery, due to the Au Mα and S Kα energy overlaps near 2.2 eV. We did find, however, that the EDX line profiles along the white arrows in Figs. 2(e) and 2(f) confirmed that the interlayer distances between W and Au atoms were similar to those directly measured in the cross-sectional ADF-STEM images.

To investigate the electronic structure modulation achieved by the S-intercalation, samples were further characterized using KPFM. The KPFM image and its line profile at the center region of a WS_2 grain after S-intercalation, yielded a contact potential difference (ΔVCPD) that was lower, by 76 mV, than that of the Au surface (Figs. 3(c) and 3(d)), whereas ΔVCPD was higher, by 32 mV, in as-grown WS_2 samples (Figs. 3(a) and 3(b)). The lower WS_2 ΔVCPD value indicated a higher work function for WS_2 than that seen for Au.

A WS_2/Au energy band diagram has been presented, as Fig. 3(e), to explain the WS_2 electronic structure modification—achieved by S-intercalation—which we observed in the KPFM results. Work functions of 4.82 eV (for Au) and 4.9 eV (for WS_2) were selected from the previous literatures [24, 25]. At the WS_2 contact with Au, in an as-grown sample, electrons were preferentially transferred from Au to WS_2, due to the lower Au work function, with the result that n-doping into WS_2 occurred. After S-intercalation, however, electrons could not be transferred to WS_2, due to the increased interfacial distance. It is acknowledged that the electronic structure of intercalated S layer has not been revealed so far. Nevertheless, our de-doping hypothesis was supported by the KPFM results.

Finally, electrochemical bubbling transfer was conducted, after S-intercalation. The optical and corresponding AFM images of WS_2 grains transferred onto the SiO_2/Si substrate show the complete transfer of WS_2 grains over the whole region [Figs. 4(a) and 4(b)], regardless of growth conditions. The characteristic Raman phonon mode and strong negative trion (X^-, at ~1.96 eV) emissions can be seen clearly in Figs. 4(c) and 4(d) [18]. Furthermore, 1 × 1 cm^2-sized WS_2 films were successfully transferred onto a SiO_2 surface (Fig. 4(e) and inset). Interestingly, only edge regions of triangular WS_2 grains were transferred without S-intercalation, as seen in Figs. 4(f) and 4(g), with the center regions remaining on the Au surface, as seen in the inset of Fig. 4(f). These results strongly supported the concept that weakening the interfacial interaction was a crucial factor in achieving a high transfer yield. Furthermore, the confocal Raman mapping images in Figs. 1(b) and 1(c) can be used as one of important indicators in determining the transfer yield—that is, the regions where the WS_2 Raman intensity was strong, were easily delaminated from the Au surface. In addition, after the WS_2 had been transferred, the Au substrate was reused for further growth processes, as shown in Fig. 5. The surface morphology remained virtually identical to a pristine Au surface and was readily available for further WS_2 growth.

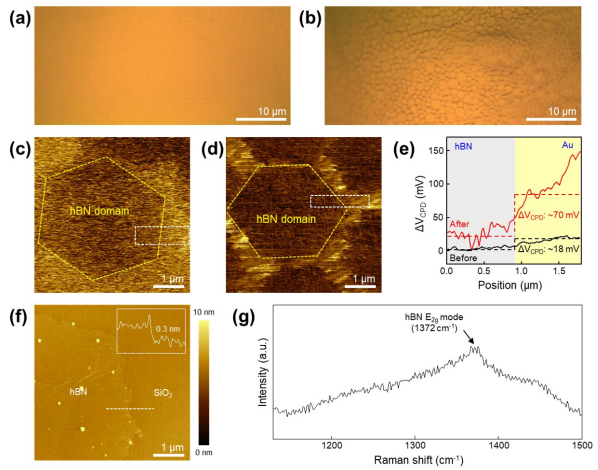

Figure 7. Optical images of (a) as-grown, and (b) S-intercalated hBN grains, on an Au substrate. KPFM potential images of hBN grains (c) before and (d) after S-intercalation. (e) Potential profiles along the white-dashed boxes in (c) and (d). (f) AFM topography image and (g) Raman spectrum respectively, of monolayer hBN grains after their transfer onto a SiO_2/Si substrate. The inset of (f) shows a height profile extracted from the white-dashed line.

To demonstrate the universal transfer of 2D materials grown on Au surfaces, molybdenum disulfide (MoS_2) and hBN were also transferred, after S-intercalation. The enhancements of $E^1{}_{2g}$ and A_{1g} phonon modes for MoS_2 after S-intercalation can be seen quite clearly in the MoS_2 confocal Raman mapping images shown in Figs. 6(a)–(c), in consistent with the change of Raman intensity seen for WS_2. AFM image of MoS_2 flakes transferred onto a SiO_2/Si substrate shows the wrinkles on the MoS_2 flakes, demonstrating successful MoS_2 transfer, as seen in Fig. 6(d). Extracted height profiles, combined with the phonon energy differences (ω) of ~19 cm^{-1} in the Raman spectrum, were further evidence of the successful transfer of a MoS_2 flake monolayer [Figs. 6(e) and 6(f)] [12].

For hBN, the optical image of as-grown hBN on Au foil shows no noticeable hBN flakes, while they are precisely visible after the S-intercalation process [Figs. 7(a) and 7(b)]. The surface potential difference between as-grown hBN flakes and Au was found to be small (~ 18 mV) in a pristine sample. This became larger (~ 70 mV) after S-intercalation [Figs. 7(c) and 7(e)]. This variation might be ascribed to the change in charge transfer behavior between hBN and the Au surface, brought about by the presence of an interfacial S layer. After a transfer of hBN flakes, the monolayer thickness of hBN and its phonon mode of E_{2g} near 1372 cm^{-1} were characterized, with the results shown in Figs. 7(f) and 7(g) [13].

4. Conclusions

In summary, we have successfully developed a method for the universal transfer of 2D materials grown on Au foil, using S-intercalation at the interface between the 2D materials and the Au surface. The S-intercalation extended the interfacial distance, as was conclusively confirmed using cross-sectional TEM. Raman spectroscopy, and KPFM provided further evidence that the S layer blocked charge transfers between the 2D materials and the Au surface. This releasing interaction enabled the successful transfer of cm-scale, monolayer WS_2 film. We anticipate that our novel transfer method will contribute to the use of SC 2D monolayers grown on Au foil in industrial applications.

Acknowledgements

This research was supported by the Institute for Basic Science (IBS-R011-D1), and by the Basic Research Program of the National Research Foundation of Korea (NRF), funded by the Ministry of Science, ICT & Future Planning (Grant Nos 2018R1A2B2002302, 2020R1A2-C1006207, and 2020R1A4A3079710). H. Y. J. acknowledges support from the Creative Materials Discovery Program through the National Research Foundation of Korea (NRF-2016M3D1A1900035). S. M. K. acknowledges support by Samsung Research Funding Incubation Center of Samsung Electronics under Project Number SRFC-MA1901-04.

References

[1] N. M. R. Peres, A. H. Castro Neto, and F. Guinea, Phys. Rev. B. 73, 241403 (2006).
[2] J. McClain and J. Schrier, J. Phys. Chem. C. 114, 14332 (2010).
[3] T. T. Tran, K. Bray, M. J. Ford, M. Toth, and I. Aharonovich, Nat. Nanotech. 11, 37 (2016).
[4] Y. Jin, M. K. Joo, B. H. Moon, H. Kim, S. H. Lee, H. Y. Jeong, and Y. H. Lee, Commun. Phys. 3, 189 (2020).
[5] M. I. Vasilevskiy, D. G. Santiago-Perez, C. Trallero-Giner, N. M. R. Peres, and A. Kavokin, Phys. Rev. B. 92, 245435 (2015).
[6] D. Manh-Ha, Y. Jin, K. C. Tuan, M. K. Joo, and Y. H. Lee, Adv. Mater. 31, 1900154 (2019).
[7] D. Fu *et al.*, J. Am. Chem. Soc. 139, 9392 (2017).
[8] L. K. Tan, B. Liu, J. H. Teng, S. Guo, H. Y. Low, and K. P. Loh, Nanoscale 6, 10584 (2014).
[9] F. Tumino, C. S. Casari, M. Passoni, V. Russo, and A. L. Bassi, Nanoscale Advances 1, 643 (2019).
[10] J. Y. Chen *et al.*, J. Am. Chem. Soc. 139, 1073 (2017).
[11] Y. Zhang *et al.*, ACS Nano 8, 8617 (2014).
[12] K. Kang, S. E. Xie, L. J. Huang, Y. M. Han, P. Y. Huang, K. F. Mak, C. J. Kim, D. Muller, and J. Park, Nature 520, 656 (2015).
[13] J. H. Park *et al.*, ACS Nano 8, 8520 (2014).
[14] X. S. Li *et al.*, Science 324, 1312 (2009).
[15] Y. Gao *et al.*, Adv. Mater. 29, 1700990 (2017).
[16] J. S. Lee *et al.*, Science 362, 817 (2018).
[17] T. A. Chen *et al.*, Nature 579, 219 (2020).
[18] S. J. Yun *et al.*, ACS Nano 9, 5510 (2015).
[19] T. H. Ly, D. J. Perello, J. Zhao, Q. M. Deng, H. Kim, G. H. Han, S. H. Chae, H. Y. Jeong, and Y. H. Lee, Nat. Commun. 7, 10426 (2016).
[20] S. H. Choi *et al.*, arXiv:2010.10097, (2020).
[21] S. M. Kim, A. Hsu, Y. H. Lee, M. Dresselhaus, T. Palacios, K. K. Kim, and J. Kong, Nanotechnology 24, 365602 (2013).
[22] S. H. Choi, C. S. Oh, S. Boandoh, W. Yang, S. M. Kim, and K. K. Kim, Appl. Sci. Converg. Tec. 28, 60 (2019).
[23] Y. Chen *et al.*, ACS Nano 12, 2569 (2018).
[24] J. H. Cha, S. J. Choi, S. Yu, and I. D. Kim, J. Mater. Chem. A. 5, 8725 (2017).
[25] V. Panchal, R. Pearce, R. Yakimova, A. Tzalenchuk, and O. Kazakova, Sci. Rep. 3, 2597 (2013).